



Cite this: *RSC Adv.*, 2019, 9, 29765

# Studies on PBFMO-*b*-PNMMO alternative block thermoplastic elastomers as potential binders for solid propellants†

Minghui Xu, <sup>\*,ab</sup> Xianming Lu,<sup>b</sup> Hongchang Mo,<sup>b</sup> Ning Liu, <sup>b</sup> Qian Zhang<sup>b</sup> and Zhongxue Ge<sup>b</sup>

An energetic polymer, poly[3,3-bis(2,2,2-trifluoro-ethoxymethyl)oxetane]glycol-*block*-poly(3-nitratomethyl-3-methyloxetane) (PBFMO-*b*-PNMMO), was synthesized using poly[3,3-bis(2,2,2-trifluoro-ethoxymethyl)oxetane]glycol (PBFMO) and poly(3-nitratomethyl-3-methyloxetane) (PNMMO) as the raw materials and toluene diisocyanate as the coupling agent *via* a prepolymer process. The structures of the energetic polymers were characterized by Fourier transform infrared spectroscopy (FT-IR), <sup>1</sup>H nuclear magnetic resonance spectrometry (<sup>1</sup>H-NMR), and <sup>13</sup>C nuclear magnetic resonance spectrometry (<sup>13</sup>C-NMR). A universal testing machine, scanning electron microscopy (SEM), differential scanning calorimetry (DSC) and thermogravimetric analysis (TGA) were used to investigate the mechanical properties and thermal behavior of PBFMO-*b*-PNMMO. The PBFMO-*b*-PNMMO-based elastomers exhibited superior mechanical properties (10.54 MPa, 723%) in comparison with PNMMO (6.18 MPa, 635%) and good compatibility with HMX and Al. The glass transition temperature (*T*<sub>g</sub>) and decomposition temperature (*T*<sub>d</sub>) were found to be −20.4 and 220 °C, respectively. The cook-off results indicated that the PBFMO-*b*-PNMMO/Al compositions could release significantly more heat than the PNMMO/Al compositions. Therefore, PBFMO-*b*-PNMMO may serve as a promising energetic binder for future solid propellant formulations.

Received 17th July 2019  
Accepted 26th August 2019

DOI: 10.1039/c9ra05517g

rsc.li/rsc-advances

## 1. Introduction

The development of high-performance composite propellants is a key area of research within current solid-state rocket propulsion. In order to attain a satisfactory performance, the replacement of the traditional inert hydroxyl-terminated polybutadiene (HTPB) binder with energetic binders has attracted an increasing interest.<sup>1–3</sup> Compared with inert binders, energetic binders contain energetic groups such as the azide group (–N<sub>3</sub>), nitrate esters (–O–NO<sub>2</sub>), nitramines (–N–NO<sub>2</sub>), and C–nitro groups (–C–NO<sub>2</sub>), which can not only impart additional energy to the formulations, but also improve the overall oxygen balance of the propellant.<sup>4,5</sup> Among the energetic binders, azide functional polymers (*viz.*, glycidyl azide polymer (GAP), poly(3,3-bis(3-azido methyl)oxetane) (PBAMO), poly((3-azido methyl)-3-methyl oxetane) (PAMMO)) and nitrate polyethers (*viz.*, poly((3-nitrate methyl)-3-methyl oxetane) (PNMMO), and

poly(glycidyl nitrate) PGN) have received widespread attention in recent decades.<sup>6–8</sup>

In the past three decades, fluoropolymers have been extensively studied in propellant or plastic-bonded explosive (PBX) formulations.<sup>9–11</sup> This is due to their high density, long-term chemical stability, low coefficients of friction, and compatibility with energetic materials, especially strong oxidative ability with metals.<sup>12–14</sup> For example, the magnesium, Teflon, and Viton (MTV) system, which was well-known in decoys and flares, has high specific infrared radiant intensity and especially large specific reaction energy of 9.4 kJ g<sup>−1</sup> in comparison to TNT and RDX with the yields of just 3.72 kJ g<sup>−1</sup> and 6.569 kJ g<sup>−1</sup>, respectively.<sup>15</sup> Therefore, fluoropolymers may serve as promising polymeric binders in metal-rich solid propellant formulations.

In this study, an energetic thermoplastic elastomer, poly[3,3-bis(2,2,2-trifluoro-ethoxymethyl)oxetane]glycol-*block*-poly(3-nitratomethyl-3-methyloxetane) (PBFMO-*b*-PNMMO), was prepared *via* a prepolymer process for metal fuel-rich solid propellant formulations. PBFMO-*b*-PNMMO consisted of poly(3-nitratomethyl-3-methyloxetane) as the soft segment and TDI-extended PBFMO as the hard segment. The molecular structure of PBFMO-*b*-PNMMO was characterized by FT-IR and NMR. The mechanical properties and thermal behavior of the elastomer were investigated by

<sup>a</sup>State Key Laboratory of Fluorine & Nitrogen Chemicals, Xi'an 710065, China<sup>b</sup>Xi'an Modern Chemistry Research Institute, Xi'an 710065, China. E-mail: mhuixu@163.com; Tel: +86 29 88291306

† Electronic supplementary information (ESI) available. See DOI: 10.1039/c9ra05517g

tensile tests, scanning electron microscopy (SEM), differential scanning calorimetry (DSC) and thermogravimetric analysis (TGA). Moreover, the cook-off test was used to evaluate the thermal performance between PBFMO-*b*-PNMMO and Al.

## 2. Experimental

### 2.1. Materials

Butane diol (BDO), dichloromethane (DCM), ethanol and 1,2-dichloroethane were purchased from Sinopharm Chemical Reagent Co. Ltd (Xi'an, China).  $\text{BF}_3$ -dimethyl ether ( $\text{BF}_3\text{OEt}_2$ ), dibutyltin dilaurate (DBTDL), and toluene diisocyanate (TDI) were supplied by Chengdu Kelong Chemical Reagents Company. BDO and  $\text{BF}_3\text{OEt}_2$  were distilled under reduced pressure prior to use. All solvents for the reactions were of analytical grade and were dried before use. [3,3-Bis(2,2,2-trifluoroethoxymethyl)oxetane]glycol (BFMO) was synthesized following the published procedure.<sup>16</sup> (3-Nitrato methyl)-3-methyl oxetane (NMMO) was synthesized as we described previously.<sup>17,18</sup>

### 2.2. Synthesis of PNMMO by cationic ring-opening polymerization

PNMMO was synthesized *via* the cationic ring-opening polymerization of NMMO using BDO as the initiator. Briefly, BDO (0.54 g, 6 mmol) and  $\text{BF}_3\text{OEt}_2$  (0.52 g, 3.6 mmol) were dissolved in DCM (20 mL) in a flame-dried 250 mL three necked flask with a mechanical stirrer, thermometer and condenser under argon atmosphere and stirred for 0.5 h. A solution of NMMO (29 g, 0.18 mol) in DCM (10 mL) was then added dropwise into the reaction solution within a period of 6 h, and the reaction was allowed to proceed for 24 h at 35 °C. Subsequently, the reaction was stopped by the addition of 2% sodium bicarbonate solution. The organic phase was washed by distilled water, dried over sodium sulphate, and filtered, and the solvent was evaporated off in vacuum at 40 °C to recover 28.2 g of PNMMO (95.5%, yield). GPC analysis:  $M_n = 4650 \text{ g mol}^{-1}$ , polydispersity index (PDI) = 1.18 (against polystyrene standards).

### 2.3. Polymerization of PBFMO

PBFMO was also synthesized through cationic ring-opening polymerization. The typical reaction procedure was as follows: BDO (0.54 g, 6 mmol),  $\text{BF}_3\text{OEt}_2$  (0.52 g, 3.6 mmol) and 26 mL DCM were charged into a three necked flask fitted with a mechanical stirrer and condenser under argon atmosphere and stirred for 0.5 h. BFMO solution (42.3 g BFMO in 10 mL DCM) was then added dropwise to the reaction flask and the polymerization was done at room temperature (30 °C) for 24 h. After polymerization, the reaction was ended by the addition of 2% sodium bicarbonate solution, followed by washing with distilled water. After evaporation of the solvent and drying under vacuum, the product was received as a white wax polymer (yield: 97.6%). GPC analysis:  $M_n = 6840 \text{ g mol}^{-1}$ , PDI = 1.22 (polystyrene standards).

### 2.4. Synthesis of PBFMO-*b*-PNMMO-based thermoplastic elastomers

PBFMO-*b*-PNMMO-based thermoplastic elastomers were synthesized using PNMMO and PBFMO as raw materials and TDI as a coupling agent *via* a prepolymer process. The typical reaction procedure was as follows: exactly 8 g PBFMO was dissolved in 15 mL freshly distilled 1,2-dichloroethane under high pure argon (99.99%) at 60 °C for 0.5 h. DBTDL (20  $\mu\text{L}$ ) and TDI (0.85 g) dissolved in 10 mL 1,2-dichloroethane was added to this mixture and stirred at 80 °C for 2 h until the hydroxyl group could not be detected. Then, PNMMO (16 g) dissolved in 15 mL 1,2-dichloroethane was added and polymerization was allowed to proceed for another 2 h at 80 °C. Thereafter, the reaction mixture was cooled to room temperature and slowly added to ethanol under stirring. The crude product precipitated out was redissolved in DCM and purified by precipitation in *n*-pentane. The recovered polymer was finally dried under vacuum at 40 °C to give a yellowish, elastomeric compound. GPC analysis:  $M_n = 53\,135 \text{ g mol}^{-1}$ , PDI = 1.82 (polystyrene standards).

### 2.5. Measurements

FTIR spectra were recorded in a Bruker Tensor 27 instrument in the range of 4000–650  $\text{cm}^{-1}$ . Nuclear magnetic resonance (NMR) spectra were measured on a Bruker 500 MHz instrument. Gel permeation chromatography (GPC) was conducted on Water GPC using tetrahydrofuran as the mobile phase and polystyrene standards for calibration. Mechanical properties including tensile strength and elongation at break of elastomer films were measured on an AG-X universal testing machine with a tensile rate of 50  $\text{mm min}^{-1}$ , and a mean value of five replicates from each film was taken. SEM was carried out on a VEGA 3 LMU scanning electron microscope (TESCAN, Czech Republic). All the elastomer films were frozen in liquid nitrogen and then snapped immediately. The fracture surfaces of the fractured films were sputtered with gold and then photographed. Differential scanning calorimetry (DSC) was carried out in a DSC Q1000 equipment at a heating rate of 10 °C  $\text{min}^{-1}$  under argon atmosphere. Thermogravimetric analysis (TGA) was performed with an SDT Q600 TGA instrument between 25 and 500 °C at a heating rate of 10 °C  $\text{min}^{-1}$ . A cook-off test was carried out on a special equipment designed by the Institute of Chemical Material, as described in Fig. 1. Samples were sealed

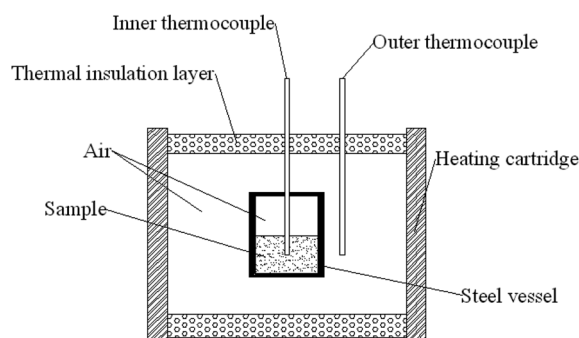


Fig. 1 Schematic geometry of cook-off test.



with a heating rate of  $1\text{ }^{\circ}\text{C min}^{-1}$  from room temperature to  $220\text{ }^{\circ}\text{C}$ , and the changes in temperatures from inner and outer thermocouples with time were recorded.

### 3. Results and discussion

#### 3.1. Synthesis of PBFMO-*b*-PNMMO-based thermoplastic elastomers

PBFMO-*b*-PNMMO-based thermoplastic elastomers were synthesized using PBFMO and PNMMO as the raw materials and TDI as the coupling agent *via* a prepolymer process; the synthetic route is described in Fig. 2. The structure of the as-synthesized PBFMO-*b*-PNMMO was confirmed by FTIR and NMR. Fig. 3 shows the FTIR spectra of PNMMO and PBFMO-*b*-PNMMO, whereas Fig. 4(A and B) depicts the  $^1\text{H}$  NMR and  $^{13}\text{C}$  NMR spectra of PBFMO-*b*-PNMMO. As shown in Fig. 3, the characteristic absorption peaks at  $1632$ ,  $1278$  and  $870\text{ cm}^{-1}$  correspond to  $-\text{O}-\text{NO}_2$  from PNMMO.<sup>19</sup> The appearance of strong peaks at  $1225$  and  $1161\text{ cm}^{-1}$  was attributed to  $-\text{CF}_3$ ,<sup>20–22</sup> the appearance of peaks at  $1412$ – $1534\text{ cm}^{-1}$  was attributed to the characteristic absorption of TDI, and the characteristic absorption peaks at  $3311$ ,  $1710$  and  $1533\text{ cm}^{-1}$  certified the formation of urethane linkage.<sup>23,24</sup> Therefore, these results gave strong evidence that the prepolymer process indeed occurred by the formation of PBFMO-*b*-PNMMO.

NMR analysis was used to determine the real composition of the as-synthesized PBFMO-*b*-PNMMO, which is shown in Fig. 4. The signals at  $3.75$  and  $4.40\text{ ppm}$  were attributed to PNMMO,<sup>19</sup> and the signal at  $3.26\text{ ppm}$  was attributed to PBFMO. The corresponding carbon signals of the methylene carbons from PBFMO and PNMMO appeared at  $73.6$  and  $75\text{ ppm}$ . The signal at  $40.4\text{ ppm}$  was attributed to the quaternary carbon atom of  $\text{C}-\text{O}-\text{NO}_2$ . The signal at  $2.18\text{ ppm}$  belonged to the methylene protons of BDO, which is the initiator of PNMMO and PBFMO; the corresponding carbon signal appeared at  $26.4\text{ ppm}$ . The signals at  $1.57\text{ ppm}$  and  $6.3$ – $8\text{ ppm}$  were attributed to the methyl protons and methine protons on the benzene rings of TDI, respectively, and the corresponding carbon signals appeared at

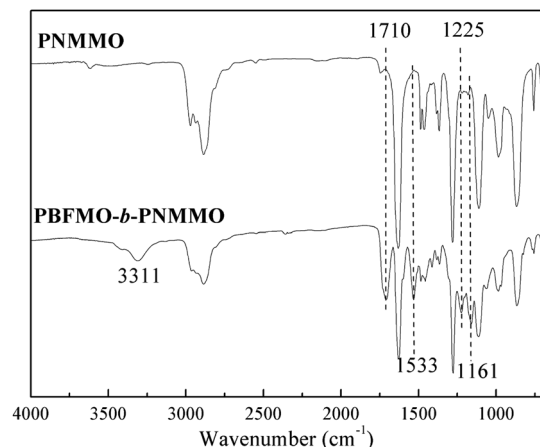


Fig. 3 FTIR spectra of PNMMO and PBFMO-*b*-PNMMO.

$17.1\text{ ppm}$  and  $120$ – $135\text{ ppm}$ . By comparing the GPC traces of PBFMO, PNMMO and PBFMO-*b*-PNMMO (Fig. S1†), a significant increase in the molecular weight was observed, which provided an experimental proof of the successful formation of PBFMO-*b*-PNMMO.

#### 3.2. Mechanical properties of PBFMO-*b*-PNMMO-based thermoplastic elastomers

The mechanical properties of the PBFMO-*b*-PNMMO- and PNMMO-based thermoplastic elastomers were evaluated *via* a universal testing machine by measuring the tensile

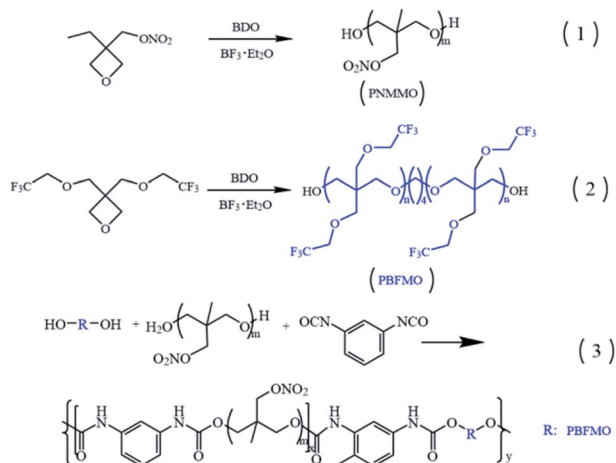


Fig. 2 The synthesis route of PBFMO-PNMMO-ETPE.

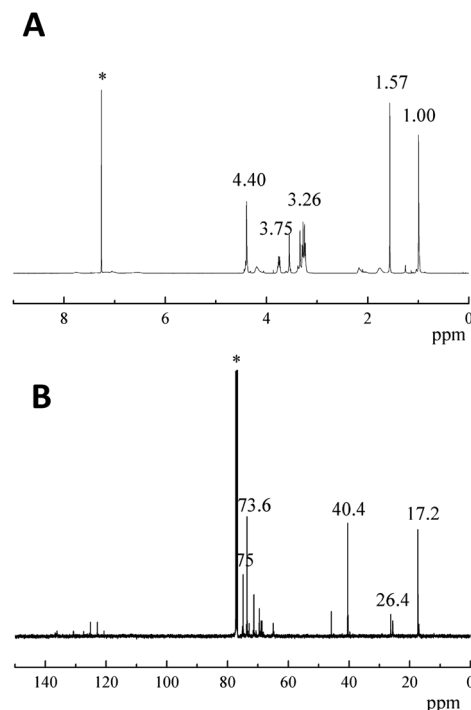


Fig. 4  $^1\text{H}$ -NMR spectrum (A) and  $^{13}\text{C}$ -NMR spectrum (B) of PBFMO-*b*-PNMMO in  $\text{CDCl}_3$ .



strength and breaking elongation.<sup>25,26</sup> An overlay of the stress–strain curves of PBFMO-*b*-PNMMO- and PNMMO-based thermoplastic elastomers is shown in Fig. 5. In contrast with the tensile strength of the PNMMO-based thermoplastic elastomers, the tensile strength of PBFMO-*b*-PNMMO significantly increased from 6.18 MPa to 10.54 MPa, while the breaking elongation increased from 635% to 723%. In theory, the change in tensile strength is usually opposite to that of breaking elongation. However, it was worth noting that the maximum value of the tensile strength for PBFMO-*b*-PNMMO was obviously higher than that for the control group, while the breaking elongation was still maintained. It is well-known that thermoplastic elastomers consist of hard segments, which act as fillers and physical crosslinks, and soft segments, which are in a rubbery state that leads to flexibility. The introduction of PBFMO having superior crystallinity provided strong cross-linking points, which inhibited the plastic deformation of the PNMMO-based soft segments and ensured an increase in the tensile strength of PBFMO-*b*-PNMMO. Meanwhile, the amounts of crosslinking points remained constant, resulting in similar values of elongation at break. Therefore, PBFMO-*b*-PNMMO exhibited satisfactory mechanical properties.

### 3.3. Fracture morphologies of PBFMO-*b*-PNMMO-based thermoplastic elastomers

To investigate the difference in the mechanical properties of the films prepared from PBFMO-*b*-PNMMO and PNMMO-based ETPE, the fracture morphologies of the films were studied by SEM. Fig. 6 shows the SEM images of the films prepared from PBFMO-*b*-PNMMO (A) and PNMMO-based ETPE (B). As shown in Fig. 6, in comparison with the observation for PNMMO-based ETPE, the fractured stripes of the gel prepared from PBFMO-*b*-PNMMO are few and scattered and the fractured surface gradually becomes smooth. Furthermore, micrographs also revealed no obvious two-phase structures in the PBFMO-*b*-PNMMO films. This indicates that PNMMO and PBFMO have good miscibility and compatibility.<sup>27</sup>

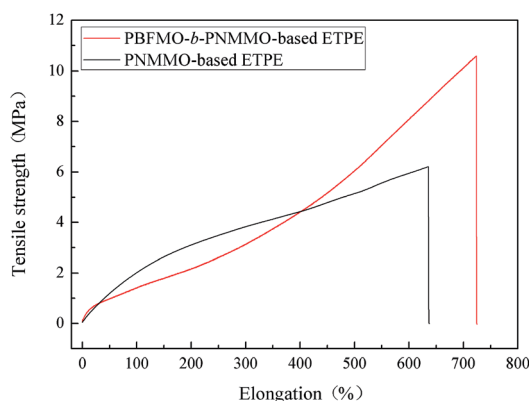


Fig. 5 Tensile testing of films prepared from PBFMO-*b*-PNMMO and PNMMO-based ETPE.

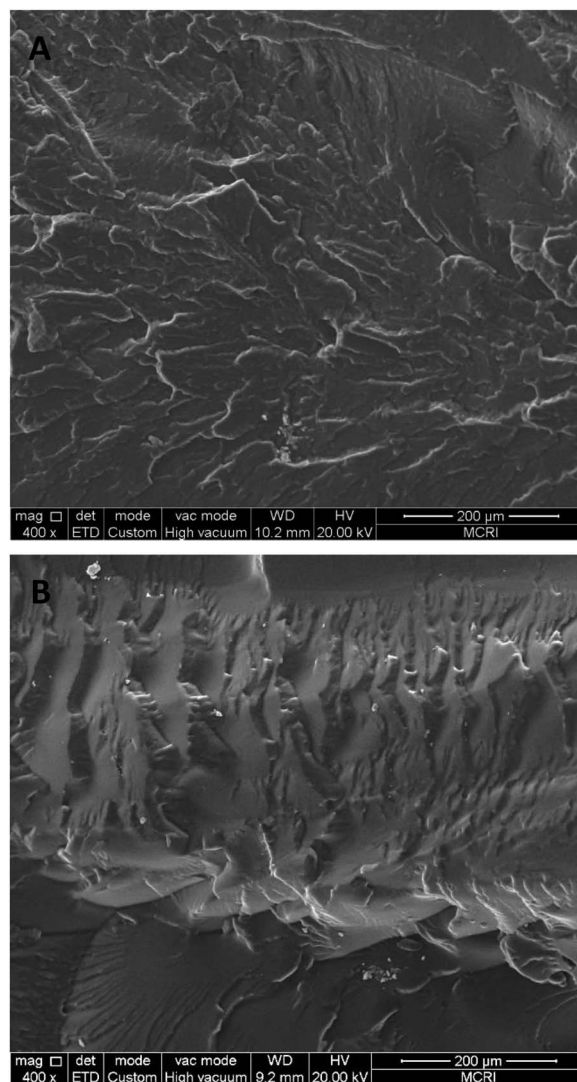


Fig. 6 SEM images for the fracture surface of the films prepared from PBFMO-*b*-PNMMO (A) and PNMMO-based ETPE (B).

### 3.4. Glass transition temperature

Glass transition temperature ( $T_g$ ) is one of the most important properties of polymeric binders because it determines the processing and application temperature range.<sup>28,29</sup> Differential scanning calorimetry (DSC) was used to measure the glass transition temperature of PBFMO-*b*-PNMMO, as shown in Fig. 7. As segmented block polyurethane, PBFMO-*b*-PNMMO is expected to possess two different  $T_g$  values. However, the curve shown in Fig. 7 exhibits only one  $T_g$  of  $-20.4$  °C. This may be due to the fact that the PNMMO and PBFMO segments are well-dispersed and blended within the films, which are also shown in Fig. 6; thus, polyurethane consists of one phase. The same phenomenon was also observed in other literatures.<sup>3,6,30</sup>

### 3.5. Thermal decomposition

It is well-known that thermal stability is a very important and crucial property for the application of energetic binders.<sup>31,32</sup>





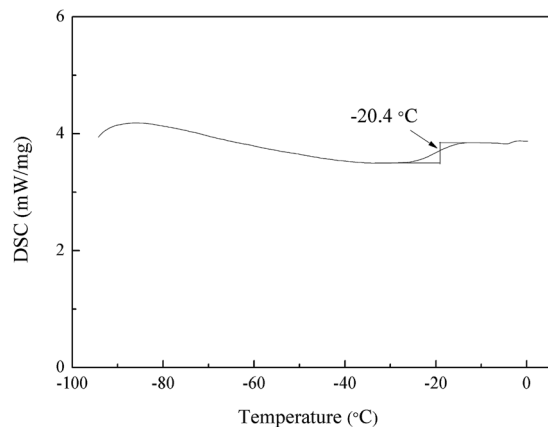


Fig. 7 Low temperature DSC curve of PBFMO-*b*-PNMMO under nitrogen.

Thus, both DSC and TGA were applied to study the thermal stability of PBFMO-*b*-PNMMO. The DSC curve (Fig. 8) shows exothermic decomposition maximum at 220 °C, which is due to the exothermic scission of nitrate esters. As shown in Fig. 9, the TGA and derivative thermogravimetry (DTG) curves of PBFMO-*b*-PNMMO also reflect excellent resistance to thermal decomposition up to 200 °C. The first weight loss temperature at 209 °C corresponded to the exothermic decomposition peak in the DSC curve. The second and third main weight losses at 304 °C and 456 °C were due to the main-chain thermal decomposition of PBFMO-*b*-PNMMO. In any case, both the DSC and TGA results confirm that PBFMO-*b*-PNMMO starts to degrade at high temperatures, thus showing satisfactory thermal stability.

### 3.6. Cook-off test

A slow cook-off test was performed to study the thermal performance of PBFMO-*b*-PNMMO and Al powders.<sup>33–35</sup> The cook-off curves of thermoplastic elastomers/Al compositions (Fig. 10) show an initial linear curves, subsequent impetuous curves and ultimately linear curves again. Generally, the integral of the outer and inner temperature curves can evaluate the

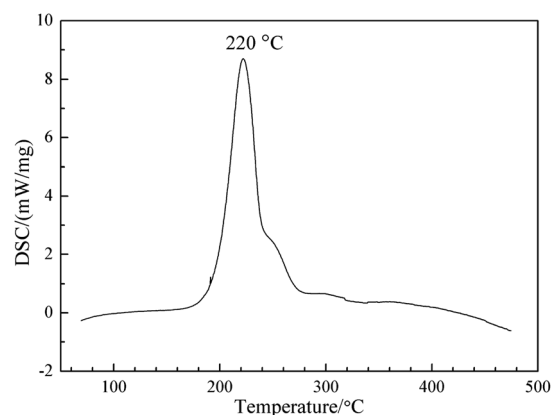


Fig. 8 DSC curve of PBFMO-*b*-PNMMO.

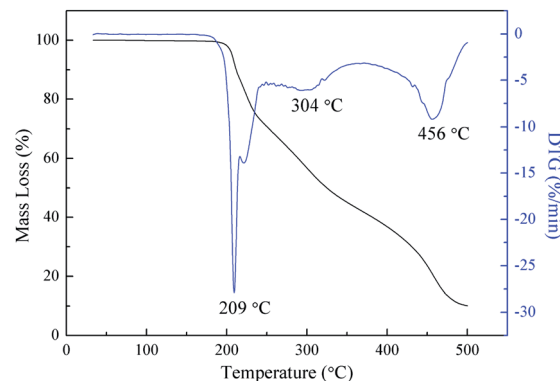


Fig. 9 TGA curves of PBFMO-*b*-PNMMO.

heat release due to the reaction between elastomers and Al. In this work, the integral of the PBFMO-*b*-PNMMO/Al group showed a remarkable increase than that of the control group. This implies that PBFMO-*b*-PNMMO can efficiently react with Al and release significantly more heat.<sup>36</sup>

### 3.7. Compatibility testing

The compatibility of binders and explosives plays a predominant role in the thermal stability of solid propellant formulations.<sup>37,38</sup> In this study, the compatibility of PBFMO-*b*-PNMMO

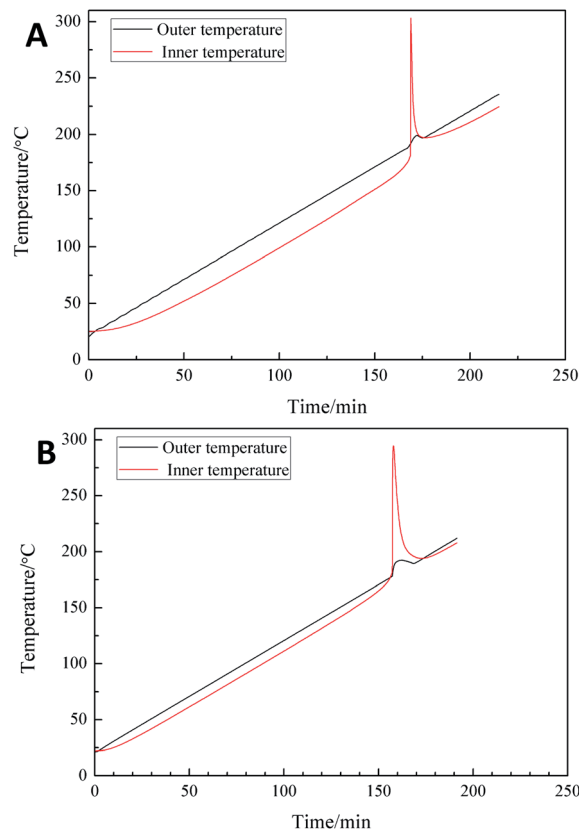


Fig. 10 Cook-off curves of PNMMO-ETPE/Al compositions (A) and PBFMO-*b*-PNMMO/Al compositions (B).



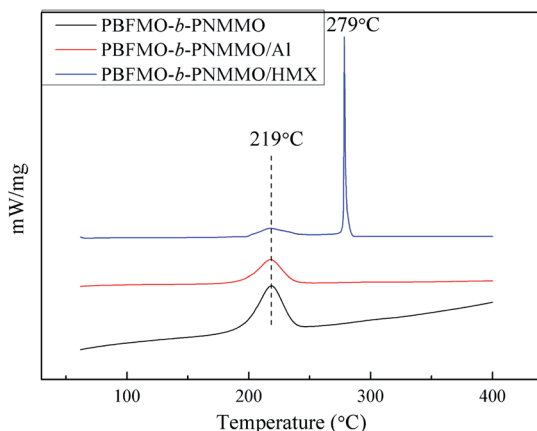


Fig. 11 DSC curves of PBFMO-*b*-PNMMO, PBFMO-*b*-PNMMO/HMX compositions and PBFMO-*b*-PNMMO/Al compositions.

with the main energetic components (*viz.*, HMX and Al) was tested by studying the effect of the contact materials on the exothermic decomposition temperature of the explosives from the DSC curves. As shown in Fig. 11, the  $\Delta T_p$  values of the binary systems, *i.e.*, PBFMO-*b*-PNMMO/HMX and PBFMO-*b*-PNMMO/Al are all less than 2 °C. The results indicate that PBFMO-*b*-PNMMO has good compatibilities with HMX and Al and can be safely used in HMX-based Al-rich propellants.

## 4. Conclusions

In this study, a novel energetic polymer, PBFMO-*b*-PNMMO, was synthesized using PNMMO and PBFMO as the raw materials and TDI as the coupling agent *via* a prepolymer process. The structure of PBFMO-*b*-PNMMO was confirmed by FTIR,  $^1\text{H}$  NMR and  $^{13}\text{C}$  NMR. The PBFMO-*b*-PNMMO films exhibited a superior mechanical performance with a tensile strength of 10.54 MPa and the corresponding breaking elongation of 723%. The DSC and TGA results indicated that PBFMO-*b*-PNMMO exhibited  $T_g$  of -20.4 °C and a good resistance to thermal decomposition up to 200 °C. The cook-off results indicated that PBFMO-*b*-PNMMO can effectively react with Al and release significantly more heat. Moreover, PBFMO-*b*-PNMMO has good compatibilities with the main components in propellants. All these results confirm that PBFMO-*b*-PNMMO might serve as a new energetic binder in propellant formulations.

## Conflicts of interest

There are no conflicts to declare.

## Acknowledgements

The authors gratefully acknowledge the financial support from the China Postdoctoral Science Foundation (2016M592851).

## Notes and references

- 1 T. Cheng, *Des. Monomers Polym.*, 2019, **22**, 54–65.

- 2 A. K. Sikder and S. Reddy, *Propellants, Explos., Pyrotech.*, 2013, **38**, 14–28.
- 3 A. Bodaghi and M. Shahidzadeh, *Propellants, Explos., Pyrotech.*, 2018, **43**, 364–370.
- 4 Y. Hu, X. Jian, L. Xiao and W. Zhou, *Polym. Eng. Sci.*, 2018, **58**, 167–173.
- 5 S. Hafner, T. Keicher and T. M. Klapoetke, *Propellants, Explos., Pyrotech.*, 2018, **43**, 126–135.
- 6 F. Abrishami, N. Zohari and V. Zeynali, *Polym. Adv. Technol.*, 2019, **30**, 640–647.
- 7 X. Wang, X. Lu, Y. Shu, H. Mo, M. Xu and N. Liu, *Fine Chem.*, 2019, **36**, 348–353.
- 8 C. Mura, S. Fruci, P. Lamia, M. Cappello, S. Filippi and G. Polacco, *J. Energ. Mater.*, 2016, **34**, 216–233.
- 9 S. K. Valluri, M. Schoenitz and E. L. Dreizin, *J. Mater. Sci.*, 2017, **52**, 7452–7465.
- 10 O. Eisenstein, J. Milani and R. N. Perutz, *Chem. Rev.*, 2017, **117**, 8710–8753.
- 11 J. H. Lee, S. J. Kim, J. S. Park and J. H. Kim, *Macromol. Res.*, 2016, **24**, 909–914.
- 12 F. Gong, H. Guo, J. Zhang, C. Shen, C. Lin, C. Zeng and S. Liu, *Propellants, Explos., Pyrotech.*, 2017, **42**, 1424–1430.
- 13 H. Yang, C. Huang and H. Chen, *J. Therm. Anal. Calorim.*, 2017, **127**, 2293–2299.
- 14 D. M. Dattelbaum, S. A. Sheffield, D. Stahl, M. Weinberg, C. Neel and N. Thadhani, *J. Appl. Phys.*, 2008, **104**, 113525–113535.
- 15 K. B. Rider, B. K. Little, S. B. Emery and C. M. Lindsay, *Propellants, Explos., Pyrotech.*, 2013, **38**, 433–440.
- 16 W. C. Jiang, Y. G. Huang, G. T. Gu, W. D. Meng and F. L. Qing, *Appl. Surf. Sci.*, 2006, **253**, 2304–2309.
- 17 H. Mo, X. Lu, L. Li, M. Chen, Y. Ji and W. Wang, *Chin. J. Energetic Mater.*, 2015, **23**, 629–632.
- 18 M. O. Hongchang, G. A. N. Xiaoxian, X. Ying and L. I. Na, *Chin. J. Explos. Propellants*, 2008, **31**, 24–27.
- 19 Q. Dong, H. Li, X. Liu and C. Huang, *Propellants, Explos., Pyrotech.*, 2018, **43**, 294–299.
- 20 X. Liu, H. Gao, X. Chen, Y. Hu, S. Pei, H. Li and Y. Zhang, *J. Membr. Sci.*, 2016, **515**, 268–276.
- 21 X. Wang, J. Hu, Y. Li, J. Zhang and Y. Ding, *J. Fluorine Chem.*, 2015, **176**, 14–19.
- 22 M. H. Xu, Z. X. Ge, X. M. Lu, H. C. Mo, Y. P. Ji and H. M. Hu, *Polym. Int.*, 2017, **66**, 1318–1323.
- 23 M. Ma and Y. Kwon, *Polym. Chem.*, 2018, **9**, 5452–5461.
- 24 A. Tanver, F. Rehman, A. Wazir, S. Khalid, S. Ma, X. Li, Y. Luo and M. H. Huang, *RSC Adv.*, 2016, **6**, 11032–11039.
- 25 I. K. Boshra, A. Elbeih and H. E. Mostafa, *Z. Anorg. Allg. Chem.*, 2019, **645**, 551–557.
- 26 Y. Yanagisawa, Y. Nan, K. Okuro and T. Aida, *Science*, 2018, **359**, 72–79.
- 27 K. Malkappa and T. Jana, *Ind. Eng. Chem. Res.*, 2013, **52**, 12887–12896.
- 28 M. Chizari and Y. Bayat, *Cent. Eur. J. Energ. Mater.*, 2018, **15**, 243–257.
- 29 Y. Wu, Z. Yi, Y. Luo, Z. Ge, F. Du, S. Chen and J. Sun, *J. Therm. Anal. Calorim.*, 2017, **129**, 1555–1562.



- 30 M. Byoung Sun and K. Seung Won, *Macromol. Res.*, 2007, **15**, 225–233.
- 31 E. Landsem, T. L. Jensen, T. E. Kristensen, F. K. Hansen, T. Benneche and E. Unneberg, *Propellants, Explos., Pyrotech.*, 2013, **38**, 75–86.
- 32 J. S. You, J. O. Kweon, S. C. Kang and S. T. Noh, *Macromol. Res.*, 2010, **18**, 1226–1232.
- 33 X. Y. Ding, Y. J. Shu, H. T. Xu and Z. Q. Chen, *Propellants, Explos., Pyrotech.*, 2018, **43**, 267–273.
- 34 W. F. Li, Y. G. Yu, R. Ye and H. W. Yang, *J. Energ. Mater.*, 2017, **35**, 265–275.
- 35 L. Chen, X. Ma, F. Lu and J. Y. Wu, *Cent. Eur. J. Energ. Mater.*, 2014, **11**, 199–218.
- 36 M. H. Xu, Z. X. Ge, X. M. Lu, H. C. Mo, Y. P. Ji and H. M. Hu, *RSC Adv.*, 2017, **7**, 47271–47278.
- 37 Y. Li, J. Li, S. Ma and Y. Luo, *Polym. Bull.*, 2017, **74**, 4607–4618.
- 38 J. F. Pei, F. Q. Zhao, H. L. Lu, X. D. Song, R. Zhou, Z.-F. Yuan, J. Zhang and J. B. Chen, *J. Therm. Anal. Calorim.*, 2016, **124**, 1301–1307.

